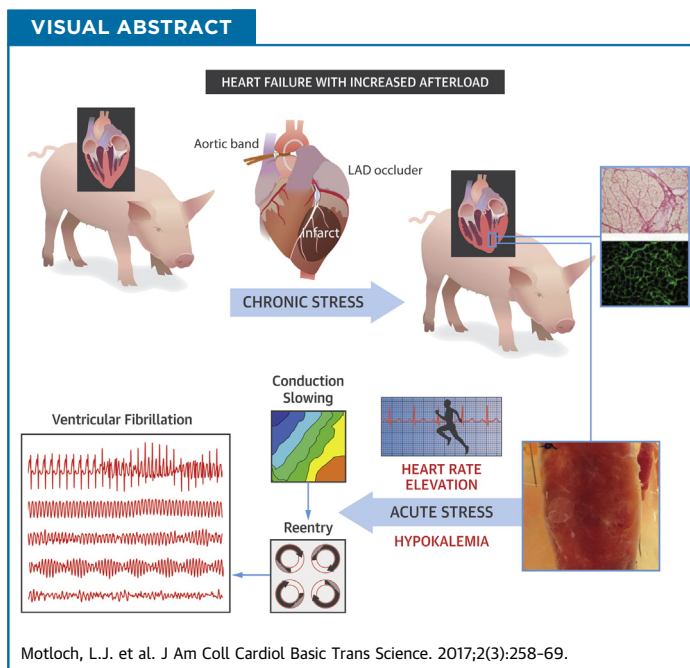**PRECLINICAL RESEARCH**

Increased Afterload Following Myocardial Infarction Promotes Conduction-Dependent Arrhythmias That Are Unmasked by Hypokalemia

Lukas J. Motloch, MD, PhD, Kiyotake Ishikawa, MD, Chaoqin Xie, MD, Jun Hu, PhD, Jaume Aguero, MD,
Kenneth M. Fish, PhD, Roger J. Hajjar, MD, Fadi G. Akar, PhD

VISUAL ABSTRACT

Motloch, L.J. et al. J Am Coll Cardiol Basic Trans Science. 2017;2(3):258–69.

HIGHLIGHTS

- Although the pathophysiological significance of hypertension in post-MI patients is established, mechanisms by which increased afterload alters the electrophysiological substrate and promotes arrhythmias after MI is unknown.

- We developed a new porcine model of MI/iAL that exhibits widespread interstitial fibrosis, increased profibrotic gene expression, and propensity to pacing-induced arrhythmias when challenged with hypokalemia.

- Investigation of the electrophysiological substrate revealed the dependence of these arrhythmias on hypokalemia-mediated conduction and not repolarization abnormalities.

- A steep negative slope of rate-dependent conduction slowing in MI/iAL is consistent with a high safety factor for propagation of slow wavefronts before onset of sustained ventricular tachycardia/ventricular fibrillation.

- Fibrosis in MI/iAL promotes the successful propagation of critically slow wavefronts leading to re-entrant arrhythmias that are unmasked by hypokalemia.

SUMMARY

Although the pathophysiological significance of resistant hypertension in post–myocardial infarction (MI) patients is established, the mechanisms by which increased afterload in that setting worsens outcome are unclear. With regard to sudden cardiac death, whether increased afterload alters the electrophysiological substrate after MI is unknown. We established a new large animal model of chronic post-MI remodeling with increased afterload that exhibits widespread deposition of fibrosis in remote areas from the anterior MI, mimicking the disease phenotype of patients with advanced ischemic heart disease. We identified the mode of initiation and mechanism of arrhythmias that were consistently unmasked by hypokalemia in this clinically relevant model. (J Am Coll Cardiol Basic Trans Science 2017;2:258–69) © 2017 The Authors. Published by Elsevier on behalf of the American College of Cardiology Foundation. This is an open access article under the CC BY-NC-ND license (http://creativecommons.org/licenses/by-nc-nd/4.0/).

Hypertension confers the greatest risk of cardiovascular-related mortality and morbidity. Despite major improvements in pharmacotherapies, the prevalence of hypertension in patients with coronary artery disease who are predisposed to myocardial infarction (MI) and sudden cardiac death remains unacceptably high (1). Although the pathophysiological significance of hypertension in post-MI patients is well established, mechanisms by which increased afterload in that setting exacerbates injury and worsens outcome are unclear. In terms of sudden cardiac death, whether (and how) increased afterload alters the electrophysiological substrate and promotes arrhythmias after MI is unknown.

We established a new large animal model of chronic post-myocardial infarction remodeling with increased afterload (MI/iAL). This model exhibits widespread deposition of fibrosis in remote areas from the anterior MI, mimicking the disease phenotype of patients with advanced ischemic heart disease. The abundant presence of diffuse fibrosis across the left ventricle in MI/iAL pigs led us to hypothesize that chronically increased afterloads in the setting of post-MI remodeling create a substrate for ventricular arrhythmias. To address this hypothesis, a systematic evaluation of the electrophysiological substrate was performed by using high-resolution optical action potential mapping in arterially perfused wedge preparations before and after challenge with hypokalemia. Hypokalemia is an ionic stressor that has been shown to exert a preferential pro-arrhythmic effect in fibrotic aged hearts (2). Post-MI pigs with increased afterload (MI/iAL) were compared with those that underwent standard MI induction without increased afterload and also with naive control animals (Ctrl). The mode of initiation and mechanism of arrhythmias that were consistently unmasked by hypokalemia were identified in this clinically relevant large animal model of MI/iAL.
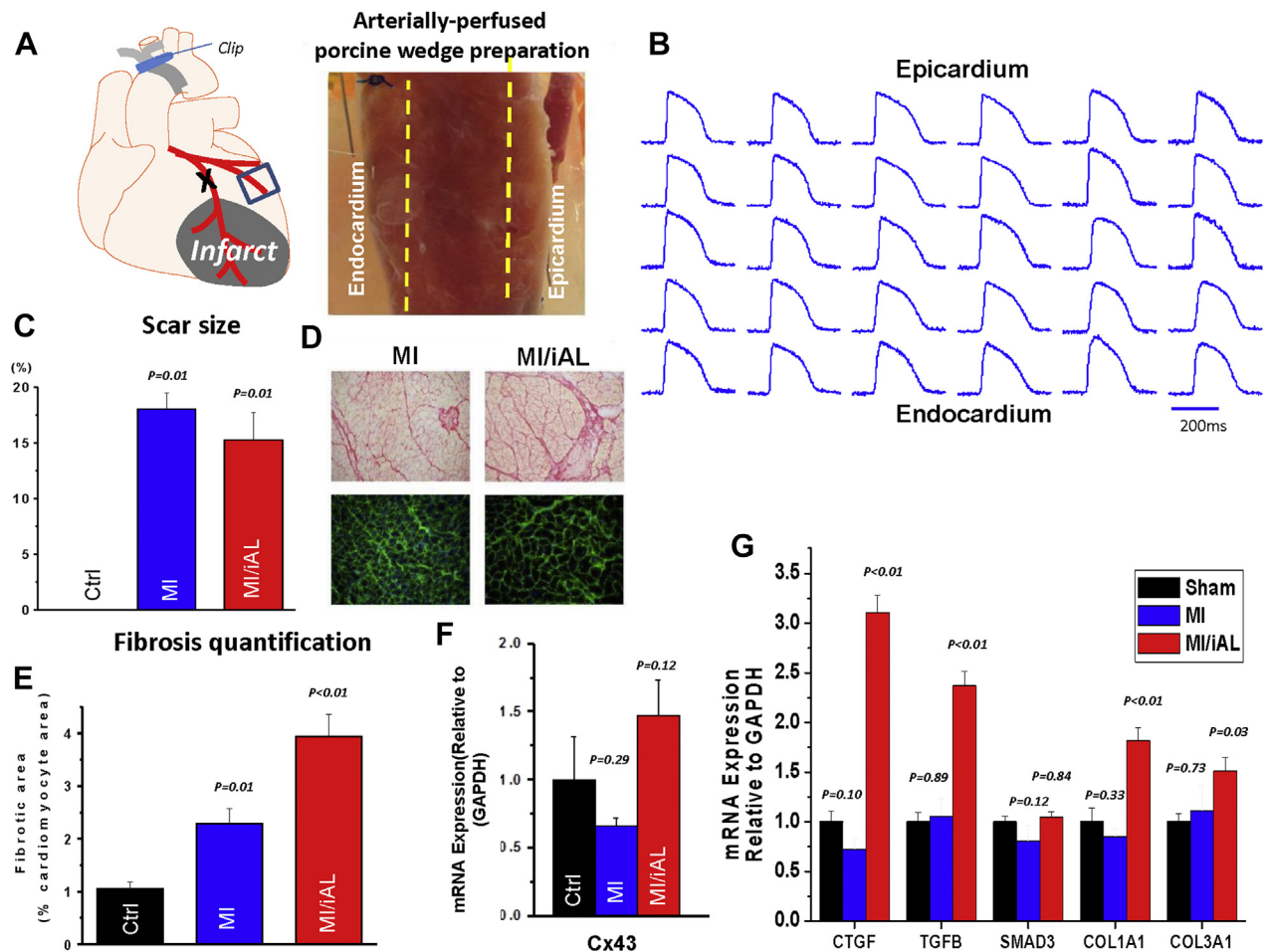
METHODS

EXPERIMENTAL PROTOCOLS. All animal handling and care complied with the Guide for the Care and Use of Laboratory Animals sponsored by the National Institutes of Health. All protocols were approved by the Institutional Animal Care and Use Committee of the Icahn School of Medicine at Mount Sinai. Twenty-five female Yorkshire pigs (approximately 20 kg) were included. Seventeen pigs were assigned to either the MI/iAL (n = 9) or the MI (n = 8) group; the Ctrl group consisted of 8 pigs that did not undergo MI induction or aortic banding. The MI/iAL and MI groups underwent MI induction on day 0. MI/iAL pigs underwent a secondary procedure of ascending aortic banding 1 month after MI. This time point was chosen to evaluate the impact of increased afterload in the setting of chronic MI, which follows the phase of active healing. Echocardiography was performed at 1, 2, and 3 months after MI. Animals were then killed, and porcine wedge preparations were isolated and arterially perfused ex vivo for optical action potential mapping studies (**Figure 1**) as described previously (3-7). Tissue specimens were collected for histological and molecular analyses, including assessment of fibrosis and fibrosis-related gene expression.

FIGURE 1 Porcine Model of MI/iAL

(A) Schematic representation and image of the arterially perfused porcine wedge preparation. **(B)** Representative transmural optical action potentials measured from across the ventricular wall of the wedge preparation. **(C)** Quantification of scar size using triphenyl-tetrazolium chloride staining. **(D)** Images of picrosirius red (fibrosis) **(top)** and wheat-germ agglutinin (hypertrophy) **(bottom)** staining showing advanced structural remodeling in hearts from the myocardial infarction model with increased afterload (MI/iAL). **(E)** Bar graphs show quantitation of interstitial collagenous tissue area against the cardiomyocyte area highlighting pronounced fibrotic remodeling in MI/iAL. **(F)** Cx43 messenger ribonucleic acid (mRNA) expression in naive control animals (Ctrl), MI/iAL, and MI animals was not different. **(G)** Quantitation of fibrosis-related gene expression at the mRNA level. Connective tissue growth factor (CTGF), transforming growth factor (TGF)-β, COL1A1, and COL3A1 but not SMAD3 ere markedly up-regulated in MI/iAL hearts compared with MI and Ctrl hearts. Three pig hearts for each group were used for the reverse transcription polymerase chain reaction analyses. GAPDH = glyceraldehyde-3-phosphate dehydrogenase.

ANIMAL MODEL OF MI/iAL. Details of the MI induction procedure have been described with visual guidance (8). Details of the aortic banding procedure have also been reported by our group (9). In brief, isoflurane-based anesthesia was initiated. A left-sided thoracotomy was performed through the third intercostal space, and a small incision was created on the pericardium. The pulmonary artery was pulled gently, and the ascending aorta was isolated and banded. The degree of stenosis was determined by evaluating the ratio of the velocity-time integral (VTI) at the left ventricular (LV) outflow tract and the site of stenosis. We aimed for a VTI ratio of 0.25 to 0.35 based on results of our recent report (9). VTI ratios <0.25 are associated with a high rate of early mortality, whereas those >0.35 are associated with minor remodeling. Using this approach, we reported a $1.7\times$ increase in fibrosis across the left ventricle.

Comprehensive transthoracic echocardiographic studies, including Doppler, 2-dimensional, and 3-dimensional echocardiography, were performed. A Philips iE33 ultrasound system (Philips Medical Systems, Andover, Massachusetts) was used to acquire echocardiographic data with a multifrequency

TABLE 1	Primers	
	Forward Primer (5′-3′)	**Reverse Primer (5′-3′)**
GAPDH	CAATGACCCCTTCATTGACC	GAAGATGGTGATGGCCTTTC
CTGF	GTGCACAGCCAAAGATTGTG	TGGTATTTGCAGCTGCTCTG
TGFB	AAAACAGGAAGGCAGTGTGG	TAGGCTGCTTTCTTGGCTTC
SMAD3	TTCTCCCTCAACCAAAGTGG	GAGCAGAAGCCATTTCTTGC
COL1A1	TTCTGCAACATGGAGACAGG	TCTTGTCCTTGGGGTTCTTG
COL3A1	TCCTCCTGGAAAGAATGGTG	TCCAGGCAAGCCTTGTAATC
Cx43	TCATGCTGGTCGTATCCTTG	TCTTTCCCTTCACACGATCC

imaging transducer. LV volumes and ejection fractions were obtained from 3-dimensional images.

TRANSMURAL OPTICAL ACTION POTENTIAL MAPPING IN PORCINE WEDGE PREPARATIONS. We previously developed the technique of transmural optical action potential mapping in arterially perfused canine wedge preparations (3-5,7). The utility of this technique has been expanded by the Efimov group to wedges from explanted human hearts (10-15).

In the present study, the same procedure was applied in the pig heart. Briefly, wedges of porcine myocardium (**Figure 1A**) were dissected from the mid apicobasal region adjacent to the anterior infarct, a region known to support post-MI arrhythmias. Wedges were arterially perfused via a secondary branch of the high lateral or posterolateral left circumflex artery, and optical mapping was performed by using a voltage-sensitive dye, di-4-ANEPPS (**Figure 1B**), as previously reported in dogs (3-7). Porcine wedge preparations were isolated from the Ctrl (n = 8 pigs; n = 12 wedges), MI (n = 5 pigs; n = 10 wedges), and MI/iAL (n = 6 pigs; n = 12 wedges) animals for detailed electrophysiological studies.

A subset of 7 Ctrl, 8 MI, and 8 MI/iAL preparations was specifically used to test the effects of hypokalemia on electrophysiological properties and arrhythmia vulnerability. For these, preparations were paced at 1.5X the diastolic threshold over a wide range of pacing rates (1.0 to 6.0 Hz in 0.5-Hz increments with pacing at each rate lasting for at least 2 min before recordings were obtained) during perfusion with normal Tyrode's solution (normokalemia, K^+ 4 mM) followed by low-K^+ solution (hypokalemia, K^+ 2 mM).
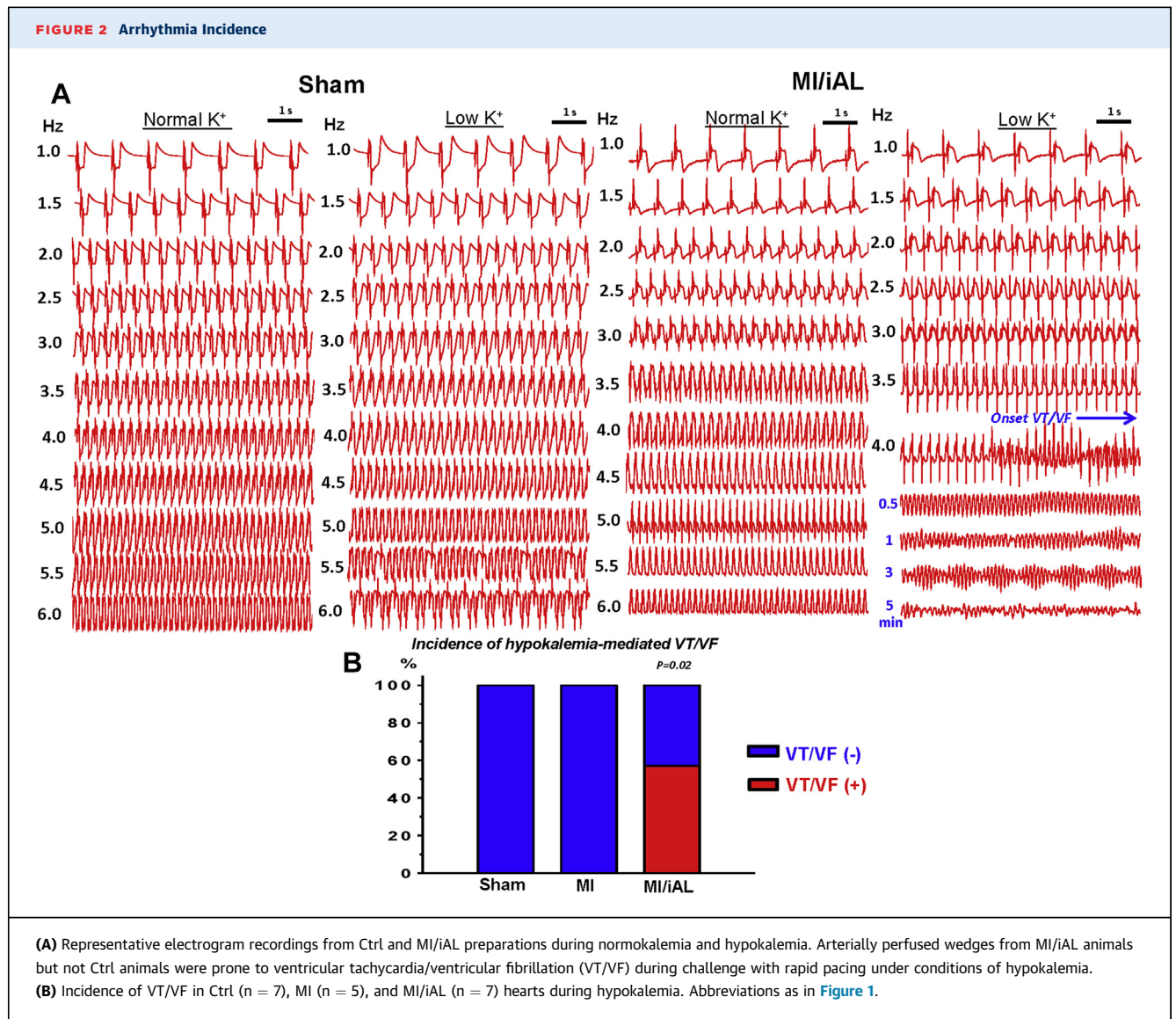
Conduction velocity (CV) was measured along the transmural axis of impulse propagation by averaging the magnitude of the velocity vectors along that direction. Basal CV (CV_b) was defined as CV during normokalemia at a pacing cycle length (PCL) of 1,000 ms. The critical CV (CV_c) was defined as the CV that was recorded at the fastest pacing rate before onset of sustained ventricular tachycardia/ventricular

fibrillation (VT/VF), loss of 1:1 pacing capture, or the end of the experimental protocol (hypokalemia, 6.0 Hz) if neither VT/VF nor loss-of-capture occurred. VT/VF was defined as pacing-induced tachyarrhythmias, which were sustained for at least 2 min. The protocol was terminated upon VT/VF occurrence.

HISTOLOGY AND MOLECULAR ANALYSES. Formalin-fixed tissue blocks from the noninfarcted myocardium were embedded in paraffin, sectioned (8 μm), mounted, and stained with wheat-germ agglutinin labeled with fluorescein isothiocyanate (for assessing hypertrophy) or picrosirius red (for assessing fibrosis). A subset of hearts was stained with triphenyl-tetrazolium chloride to highlight the scar area relative to viable tissue, and the size of the scar was assessed by using digital planimetry.

REVERSE TRANSCRIPTION–POLYMERASE CHAIN REACTION. Total ribonucleic acid (RNA) was isolated by using acid guanidinium thiocyanate-phenol-chloroform extraction by 1 ml TRIzol Reagent (Life Technologies, Carlsbad, California). Total RNA was reverse transcribed into first-strand complementary deoxyribonucleic acid by using a High-Capacity cDNA Reverse Transcription Kit with RNase inhibitor (Applied Biosystems, Foster City, California) with random primers. Real-time polymerase chain reaction (PCR) was performed by using the 7500 Fast Real-Time PCR System and Fast SYBR green PCR master mix (Applied Biosystems) in duplicate. High-resolution melting curves were generated to confirm the specificity of the PCR products. After rectification by the passive reference dye ROX within the master mix, the threshold cycle values were determined by using SDS version 1.5.1 (Applied Biosystems). The relative messenger RNA expression levels of a given gene were evaluated by the $2^{-\Delta CT}$ method. Levels of messenger RNA of each target gene were normalized to those of the internal control (glyceraldehyde-3-phosphate dehydrogenase). Primers used in this study are shown in **Table 1**.

STATISTICAL ANALYSIS. N and n refer to the numbers of pigs and arterially perfused wedge preparations, respectively. Hemodynamic measurements (performed in animals) are expressed as mean ± SD; electrophysiological measurements (performed in wedges) are expressed as mean ± SEM. Differences between groups were evaluated by using chi-square testing for discrete variables (presence vs. absence of VT/VF, maintenance vs. loss of 1:1 capture). For continuous variables, the Shapiro-Wilk test was applied to test for normal distribution of data for a given metric in a given group. If data were normally distributed, the Student *t* test or analysis of variance

FIGURE 2 Arrhythmia Incidence

(A) Representative electrogram recordings from Ctrl and MI/iAL preparations during normokalemia and hypokalemia. Arterially perfused wedges from MI/iAL animals but not Ctrl animals were prone to ventricular tachycardia/ventricular fibrillation (VT/VF) during challenge with rapid pacing under conditions of hypokalemia. (B) Incidence of VT/VF in Ctrl (n = 7), MI (n = 5), and MI/iAL (n = 7) hearts during hypokalemia. Abbreviations as in Figure 1.
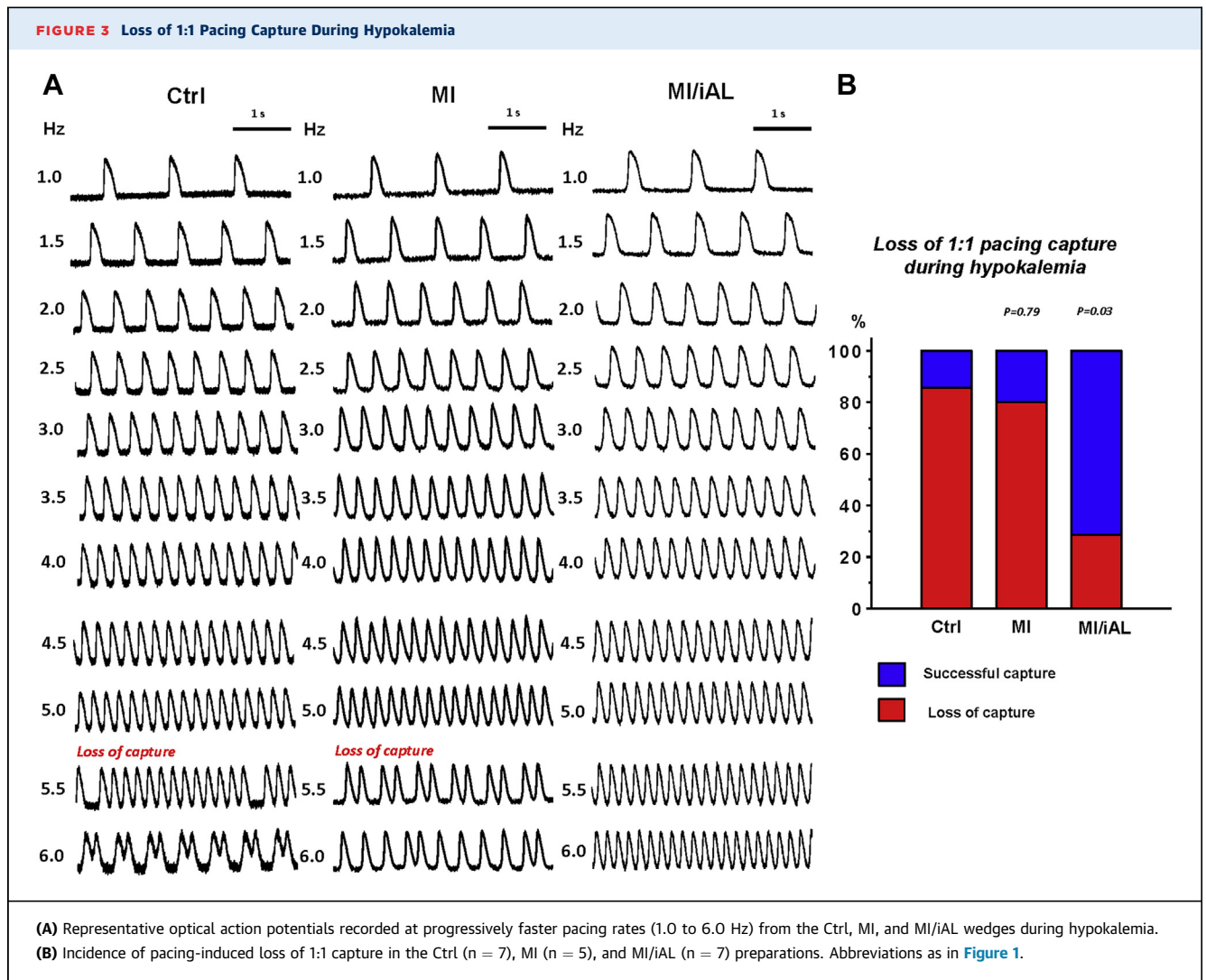
(ANOVA) followed by Tukey's test were performed. The unpaired Student *t* test was used to compare differences between 2 groups. For multiple comparisons, 1-way ANOVA followed by post hoc Tukey's test was calculated. If normal distribution could not be confirmed, Kruskal-Wallis or Mann-Whitney *U* tests were applied. A p value <0.05 was considered statistically significant. The total number of preparations used in each figure is indicated in the corresponding figure legend. Statistical analyses were performed by using SPSS version 22 (IBM SPSS Statistics, IBM Corp., Armonk, New York).

RESULTS

Successful aortic banding in MI/iAL animals was confirmed by echocardiography: the VTI ratio was markedly decreased compared with MI animals that were not subjected to aortic banding (0.29 ± 0.08 vs. 0.73 ± 0.11; p < 0.001). Surprisingly, the extent of mechanical dysfunction in MI/iAL and MI animals was similar as both groups exhibited a comparable decrease in the maximal rate of rise of left ventricular pressure (dP/dt_{max}) (MI/iAL: 1,935 ± 749 mm Hg/s; MI: 2,111 ± 661 mm Hg/s; Ctrl: 2,855 ± 814 mm Hg/s; ANOVA, p = 0.10 with post hoc MI/iAL vs. MI: p = 0.65) and an increase in LV end-diastolic pressure (MI/iAL: 20.7 ± 5.8 mm Hg; MI: 19.8 ± 4.8 mm Hg; Ctrl: 12.9 ± 3.8 mm Hg; ANOVA, p = 0.02 with post hoc MI/iAL vs. MI: p = 0.75) compared with their Ctrl counterparts.

Unlike mechanical function, structural remodeling was significantly more advanced in MI/iAL animals compared with MI animals despite a comparable scar

FIGURE 3 Loss of 1:1 Pacing Capture During Hypokalemia

(A) Representative optical action potentials recorded at progressively faster pacing rates (1.0 to 6.0 Hz) from the Ctrl, MI, and MI/iAL wedges during hypokalemia. (B) Incidence of pacing-induced loss of 1:1 capture in the Ctrl (n = 7), MI (n = 5), and MI/iAL (n = 7) preparations. Abbreviations as in **Figure 1**.

size (**Figure 1C**). Picrosirius red staining revealed increased (by approximately 2-fold) interstitial fibrosis in the MI/iAL animals compared with the MI animals (**Figures 1D and 1E**). In addition, the expression of multiple profibrotic genes and fibrosis markers, including connective tissue growth factor, transforming growth factor-β, Col1A1, and Col3A1, were markedly (1.5-fold to 3-fold; p < 0.01) up-regulated in MI/iAL animals compared with MI and Ctrl animals (**Figure 1G**). Cx43 messenger RNA expression exhibited a trend toward increased levels in MI/iAL animals and decreased levels in MI animals compared with Ctrl animals (**Figure 1F**).

INCIDENCE OF VT/VF IN MI/iAL. Because hearts of MI/iAL animals exhibited widespread deposition of interstitial fibrosis and a pro-fibrotic molecular signature, we hypothesized that they were prone to arrhythmias, particularly during the ionic stress of

hypokalemia, which was shown by Bapat et al. (2) to preferentially impact fibrotic hearts. To address this situation, arterially perfused porcine wedge preparations from Ctrl, MI, and MI/iAL animals were subjected to a wide range of pacing rates under conditions of normokalemia and hypokalemia. Although none of the Ctrl preparations (0 of 7) exhibited onset of VT/VF during normokalemia or hypokalemia, 38% (3 of 8; MI vs. Ctrl: p = 0.07) and 63% (n = 5 of 8; Ctrl vs. MI/iAL: p = 0.01) of MI and MI/iAL preparations, respectively, were prone to VT/VF. Importantly, the majority (4 of 5) of VT/VF episodes in MI/iAL preparations occurred during hypokalemic stress. In sharp contrast, none (0 of 5) of the MI hearts that underwent hypokalemia challenge were prone to arrhythmias (**Figure 2,** Supplemental Table 1). These observations highlight a unique pro-arrhythmic response of MI/iAL hearts to hypokalemia.
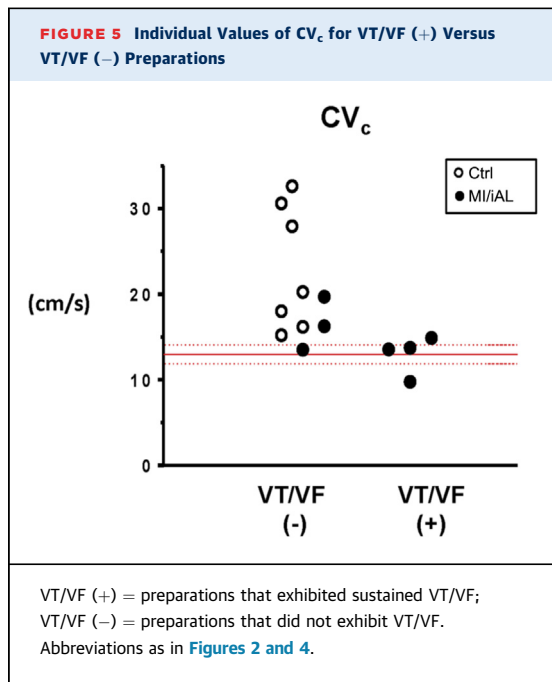
FIGURE 4 Basal and Critical Conduction Velocities
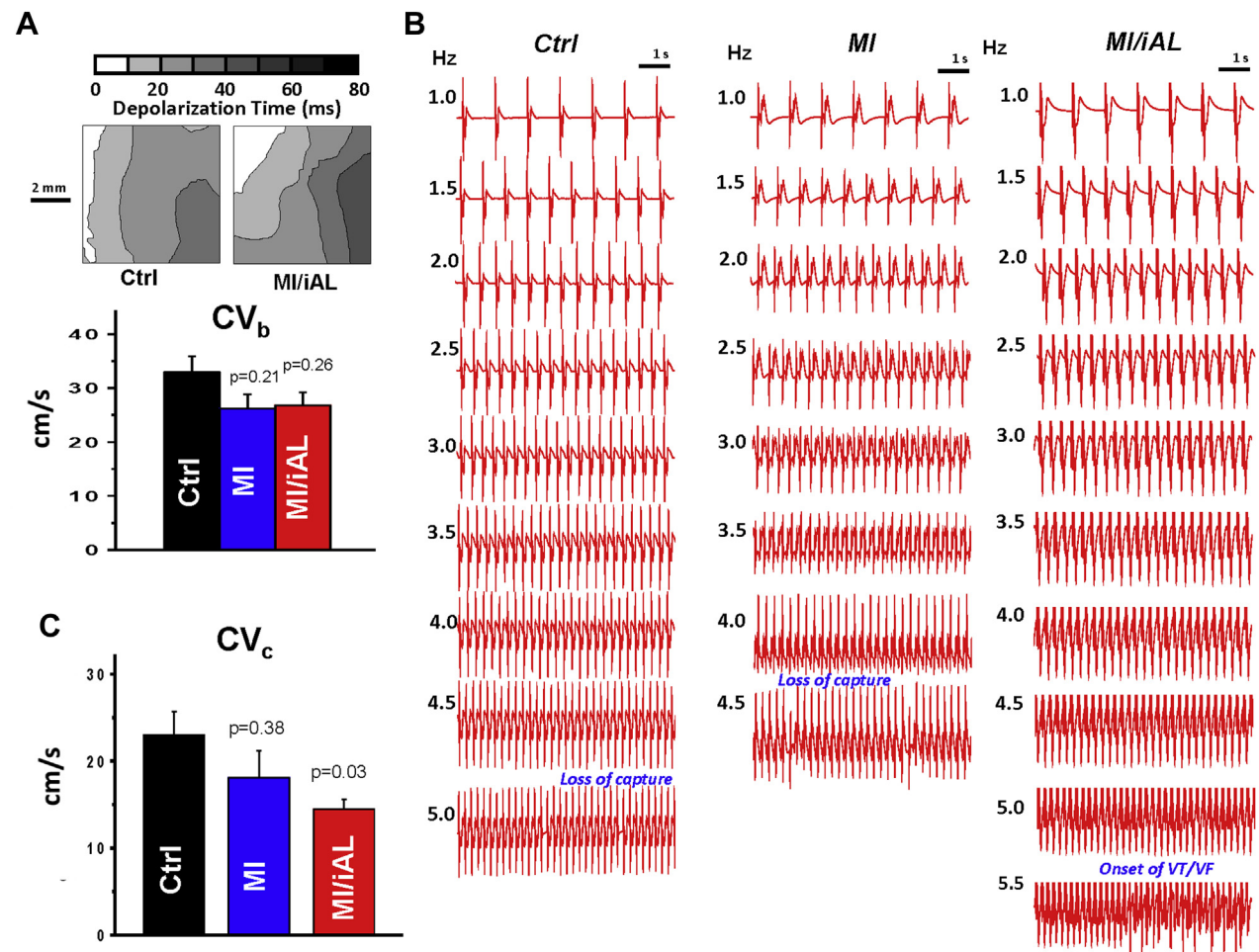
(A) Representative depolarization isochrone maps from Ctrl and MI/iAL preparations at baseline (normokalemia, pacing cycle length 1,000 ms). Comparison of basal conduction velocity (CV$_b$) in the Ctrl, MI, and MI/iAL preparations (Ctrl: n = 11; MI: n = 9; and MI/iAL: n = 10). No significant differences in CV$_b$ were found between the MI or MI/iAL preparations compared with the Ctrl preparations. **(B)** Representative electrogram tracings recorded at a wide range of pacing rates in the Ctrl, MI, and MI/iAL preparations during hypokalemia challenge. **(C)** Comparison of average critical conduction velocity (CV$_c$) (Ctrl: n = 7; MI: n = 4; and MI/iAL: n = 7) indicating significantly decreased levels in the MI/iAL group. Abbreviations as in **Figures 1 and 3**.

Hypokalemia is known to promote arrhythmias in part by impairing repolarization, prolonging the action potential duration (APD), and forming afterdepolarization-mediated triggers. We measured the average endocardial, mid-myocardial, and epicardial APDs during normokalemia and hypokalemia (Supplemental Figure 1). Hypokalemia resulted in a comparable prolongation of APD across all muscle layers of all groups. Moreover, quantification of APD heterogeneity as indexed by the range and SD of APD values across the transmural wall revealed no significant differences between groups, neither during normokalemia nor hypokalemia. As such, these data discount a major role for APD prolongation or repolarization heterogeneity in the hypokalemia-mediated arrhythmias that were unique to the MI/iAL group.

We instead uncovered an unexpected effect on excitability in the MI/iAL group compared with the MI and Ctrl groups (Figure 3). Although an increase in pacing rate during hypokalemia resulted in the loss of 1:1 pacing capture in 86% of Ctrl wedges and 80% of MI wedges, the same challenge resulted in loss-of-capture of only 29% of preparations from MI/iAL animals, which instead were prone to pacing-induced VT/VF (Figure 2). These data highlight an intrinsically unique response of MI/iAL wedges to conditions that lower excitability, namely the combination of hypokalemia and rapid pacing.

FIGURE 5 Individual Values of CV_c for VT/VF (+) Versus VT/VF (−) Preparations

VT/VF (+) = preparations that exhibited sustained VT/VF; VT/VF (−) = preparations that did not exhibit VT/VF. Abbreviations as in **Figures 2 and 4**.

RATE-DEPENDENT CONDUCTION IN MI/iAL. We next hypothesized that conduction abnormalities may be mechanistically involved in the pathogenesis of arrhythmias in this model. To address this theory, we began by measuring the basal conduction velocities (CV_b) in the Ctrl, MI, and MI/iAL preparations. Despite a trend toward reduced CV_b in the MI and MI/iAL preparations relative to the Ctrl preparations, differences did not reach statistical significance (**Figure 4A**). Because the arrhythmias in this model were elicited by progressive elevation in pacing rate during challenge with hypokalemia, we compared CV values measured just before the onset of VT/VF or the loss of 1:1 capture in Ctrl, MI, and MI/iAL preparations (**Figure 4B**). CV measured under these conditions of low excitability was defined as the critical CV (CV_c) because it represented the near final measurable level before arrhythmias were initiated or the initial loss of excitability encountered. Unlike CV_b, CV_c was significantly (p = 0.03) lower in MI/iAL preparations compared with Ctrl preparations (**Figure 4C**). In contrast, MI preparations exhibited relatively preserved (p = 0.38) CV_c compared with Ctrl hearts. Of note, preparations that were prone to hypokalemia-mediated VT/VF were associated with a very narrow distribution of CV_c values that clustered at approximately 13 cm/s (**Figure 5**). In sharp contrast, a much wider distribution of CV_c values ranging from 15 to 35 cm/s was evident in arrhythmia-free or VT/VF (−) preparations.
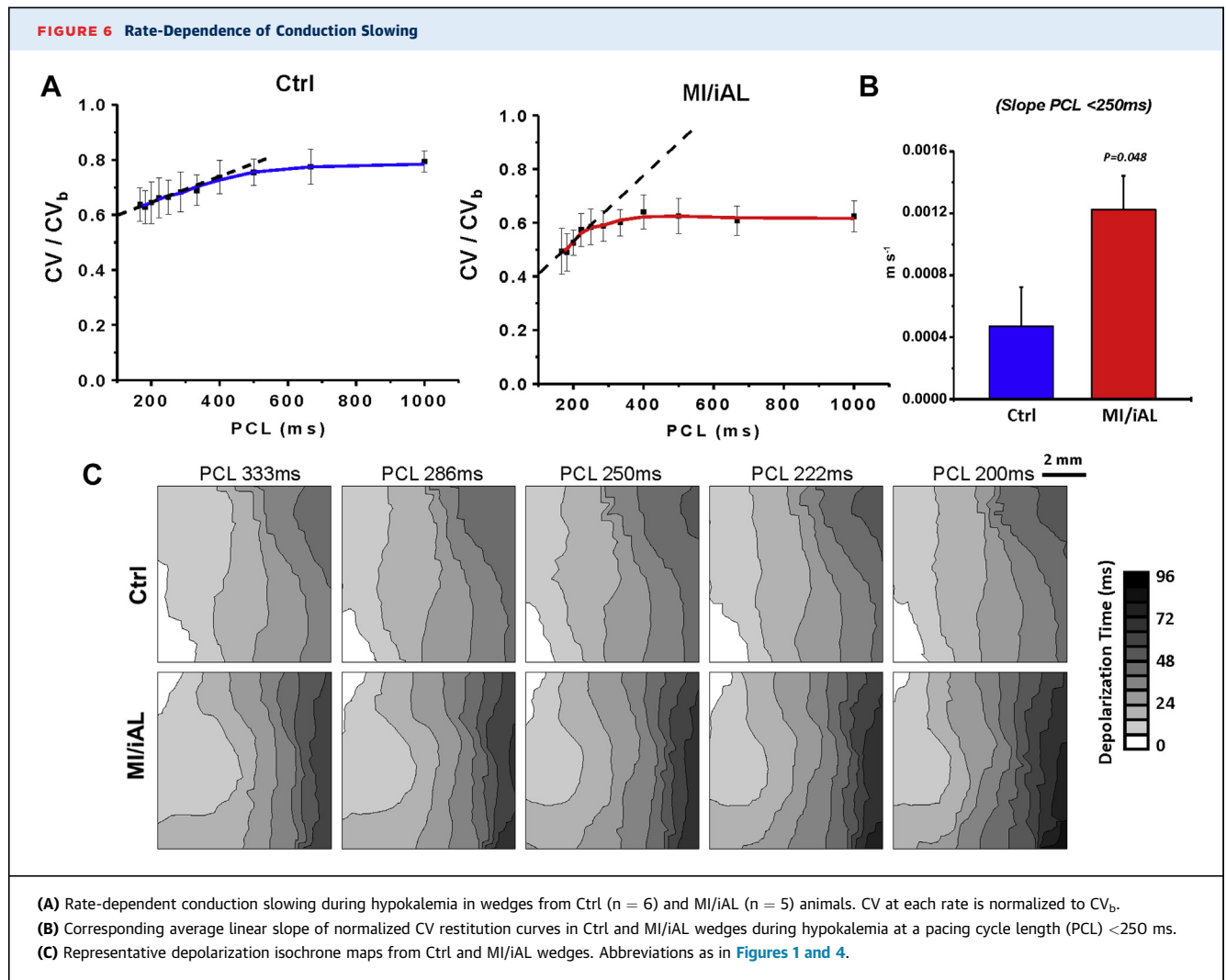
The rate-dependent kinetics of CV in Ctrl and MI/iAL preparations during hypokalemia were next examined. To determine CV at very fast rates in Ctrl hearts, 1:1 pacing capture could be reestablished by increasing the pacing voltage once the initial loss-of-capture occurred. As shown in **Figures 6A to 6C**, major differences were found in the normalized CV restitution curves between the Ctrl and MI/iAL preparations during hypokalemia. In particular, although Ctrl hearts exhibited a shallow slope of the CV restitution curves at PCL <250 ms, MI/iAL preparations were associated with a significantly steeper slope, indicating a progressively decreasing CV profile over these rates. A linear fit of the normalized CV vs cycle length relationship over the relevant rates that precipitated VT/VF (PCL <250 ms) revealed a significantly (p < 0.05) greater negative slope in MI/iAL compared with Ctrl (**Figure 6B**).

Conduction slowing is an established mechanism that promotes re-entrant arrhythmias (5,11). Optical imaging in MI/iAL preparations revealed areas of functional conduction block and circuits of re-entrant excitation underlying hypokalemia-mediated VT/VF (Supplemental Video 1). A biophysical requirement for re-entrant excitation to persist entails a short cardiac wavelength (λ) that must be smaller than the path length of the circuit. We measured λ (the product of APD and CV) under conditions of impaired excitability that led to VT/VF (λ_c). As shown in **Figures 7A and 7B**, λ_c was significantly shorter in MI/iAL hearts compared with Ctrl hearts, reaching levels smaller than the physical dimensions of the wedge preparation. Of note, λ_c in the majority (5 of 7) of the MI/iAL preparations (but not the Ctrl [1 of 7] preparations) was <2.0 cm, consistent with increased vulnerability to re-entrant arrhythmias.

DISCUSSION

In the present study, a chronically elevated afterload in the setting of post-MI remodeling was associated with a major rise in interstitial fibrosis and a pro-fibrotic program (**Figure 1**). These structural abnormalities were associated with increased LV stiffness (not shown) and a vulnerable electrophysiological substrate that was unmasked by hypokalemia (**Figure 2**).

Specifically, we found that the mode of arrhythmia initiation was invariably related to conditions that reduced excitability (**Figures 2 and 3**). Indeed, the majority of arrhythmias were encountered during rapid pacing under hypokalemic conditions. This finding may be of clinical relevance considering the common use of diuretic agents in patients with

FIGURE 6 Rate-Dependence of Conduction Slowing

(A) Rate-dependent conduction slowing during hypokalemia in wedges from Ctrl (n = 6) and MI/iAL (n = 5) animals. CV at each rate is normalized to CV_b.
(B) Corresponding average linear slope of normalized CV restitution curves in Ctrl and MI/iAL wedges during hypokalemia at a pacing cycle length (PCL) <250 ms.
(C) Representative depolarization isochrone maps from Ctrl and MI/iAL wedges. Abbreviations as in **Figures 1 and 4**.
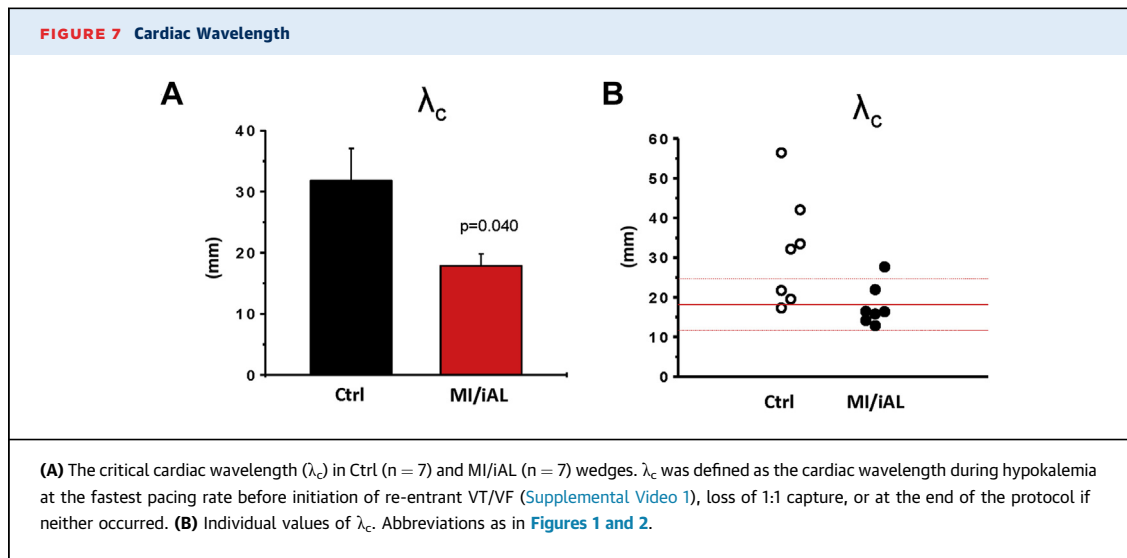
chronic MI and arterial hypertension. Of note, 10% to 40% of patients treated with diuretic agents exhibit hypokalemia along with its pathological manifestations (16). Furthermore, diuretic agents increase the risk of sudden cardiac death in patients with heart failure and arterial hypertension (17,18).

The present model of chronic MI/iAL allowed us to examine the mechanism underlying hypokalemia-mediated arrhythmias in the setting of increased afterload. Although hypokalemia promotes a host of electrophysiological instabilities that render the heart more vulnerable to arrhythmias, including APD prolongation and enhanced automaticity (19), the mechanism underlying its pronounced effect in diseased hearts compared with normal hearts is unclear. Our present findings highlight the importance of hypokalemia-related conduction slowing rather than repolarization instability in arrhythmias in a pre-clinical model of advanced structural heart

disease. Of note, our experimental measurements of CV_c (averaging 23 cm/s) in preparations from Ctrl animals, which reflect the near minimum CV that is supported by normal cardiac tissue before loss-of-capture emerges, were consistent with the minimal attainable CV computed by Shaw and Rudy before onset of conduction failure (17 cm/s) in their in silico linear fiber model of normal guinea pig myocytes (20,21).

The present experimental protocol permitted the evaluation of CV levels even after the initial loss of 1:1 capture in arrhythmia-free preparations because reliable pacing could be re-established by increasing the stimulus voltage. A major unexpected finding was that CV had already reached a near "minimal" level once the initial loss-of-capture occurred. A further increase in pacing rate did not significantly decrease CV thereafter. The unique rate-dependent kinetics of CV that we report in Ctrl preparations during conditions of low excitability (rapid pacing and hypokalemia) are

FIGURE 7 Cardiac Wavelength

(A) The critical cardiac wavelength (λ_c) in Ctrl (n = 7) and MI/iAL (n = 7) wedges. λ_c was defined as the cardiac wavelength during hypokalemia at the fastest pacing rate before initiation of re-entrant VT/VF (Supplemental Video 1), loss of 1:1 capture, or at the end of the protocol if neither occurred. (B) Individual values of λ_c. Abbreviations as in **Figures 1 and 2**.

marked by a flat slope of the steady-state CV restitution curve at PCL <250 ms (**Figure 6**). This unexpected finding is consistent with the notion that the minimal CV in these preparations failed to reach critically slow levels that promote arrhythmias. In sharp contrast, MI/iAL wedges exhibited a markedly lower incidence of loss-of-capture and a steeper slope of rate-dependent CV slowing during hypokalemia challenge. This outcome, in turn, resulted in a progressive decrease in CV that likely culminated in the initiation and maintenance of re-entrant activation.

Another finding that prompted us to investigate the arrhythmic phenotype of MI/iAL animals was the widespread proliferation of diffuse interstitial fibrosis and the increased expression of multiple fibrosis markers (**Figure 1**). Although fibrosis in this model did not cause conduction slowing under basal conditions, it likely facilitated the successful propagation of critically slow wavefronts under conditions of low excitability (hypokalemia and rapid pacing) that failed to generate propagating wavefronts in Ctrl and MI tissues. Of note, Rudy et al. (20,21) illustrated (using computational modeling) the concept of the "safety factor" of conduction, a dimensionless parameter that reflects the margin of safety with which the action potential propagates relative to the minimum requirements for sustained conduction. In particular, they showed that the safety factor is increased when the loss of nonexcitatory current to electro-tonic interactions is diminished. Our present findings in this clinically relevant animal model of MI/iAL provide experimental credence to these theoretical predictions and extend them to situations in which conduction is adversely affected by a

profibrotic program that increases extracellular resistivity as opposed to Cx43 down-regulation.

To further explore if differences in the rate dependence of CV slowing during hypokalemia promoted the incidence of VT/VF in MI/iAL, λ was calculated at baseline and during conditions leading up to the initiation of VT/VF. At baseline, arterially perfused wedges from Ctrl and MI/iAL animals exhibited comparable λ (not shown). In contrast, hypokalemia and rapid pacing caused a more pronounced shortening of λ in MI/iAL compared with Ctrl preparations (**Figure 7**), likely explaining their propensity for re-entrant excitation (Supplemental Video 1).

CLINICAL IMPLICATIONS. In the present study, VT/VF was induced by rapid pacing by using frequencies that are commonly applied during antitachycardia pacing therapy in clinical practice. Antitachycardia pacing is implemented to reduce the frequency of high-energy shocks and therefore to improve the quality of life of patients with an implantable cardioverter-defibrillator (22). However, this therapy carries the risk of VT initiation and/or acceleration and may increase mortality in patients. Indeed, our present findings provide a mechanistic framework that explains the pro-arrhythmic effects of antitachycardia pacing in patients with increased afterload. In addition, rapid ventricular pacing is also implemented in the context of the transcatheter aortic valve implantation procedure (23). In a patient population with increased afterload, a history of MI, and systolic dysfunction, rapid pacing during transcatheter aortic valve implantation may promote the incidence of intraoperative VT/VF.

Together, the present findings emphasize the need to closely monitor serum K^+ levels in patients with hypertension. Although hypokalemia lowers diastolic excitability, hyperkalemia or treatment of MI/iAL patients with sodium channel blockers may carry a comparable risk by also impairing excitability.

STUDY LIMITATIONS. Our ex vivo approach for evaluating arrhythmia susceptibility was based on challenge of preparations with rapid pacing. Indeed, the rapid rates that elicited hypokalemia-mediated VT/VF in the wedge preparation do not reflect the typical average heart rates in patients. Having said that, the proposed mechanism for arrhythmia initiation in this model, which is based on the shortening of the cardiac wavelength below the path length of a re-entrant circuit, is likely to be underestimated in the porcine wedge preparation owing to its small dimensions (approximately $3 \times 1.5 \times 1.5$ cm) relative to that of the intact heart. As such, pacing-induced arrhythmias in the intact failing heart are expected to be encountered at slower rates than the ones reported in the wedge preparations. Moreover, closely coupled premature ventricular contractions that are frequently observed in failing hearts (especially during hypokalemia) are likely to be associated with similar conduction patterns and arrhythmia risk, as shown here for rapid pacing. This challenge, however, was not directly tested in our studies.

Another key limitation is the absence of adrenergic signaling in the ex vivo perfused preparations. Of note, Lang et al. (14) showed in their arterially perfused wedge preparations from failing human hearts the importance of selective α_2-adenoreceptor activation in the exacerbation of electrical remodeling and arrhythmias. This factor was not accounted for in our experimental design.

CONCLUSIONS

Chronically increased afterload following myocardial infarction causes widespread proliferation of diffuse fibrosis across the ventricle. This advanced structural remodeling program promotes conduction-dependent arrhythmias that are unmasked by hypokalemia at rapid heart rates.

ADDRESS FOR CORRESPONDENCE: Dr. Fadi G. Akar, Cardiovascular Research Center, Icahn School of Medicine at Mount Sinai, One Gustave L. Levy Place, Box 1030, New York, New York 10029-6574. E-mail: fadi.akar@mssm.edu.

PERSPECTIVES

COMPETENCY IN MEDICAL KNOWLEDGE: A chronically elevated afterload in the setting of post-MI remodeling was associated with a major rise in interstitial fibrosis and a pro-fibrotic gene program. These structural abnormalities produced a vulnerable electrophysiological substrate that was unmasked by hypokalemia. The importance of hypokalemia-related conduction slowing and reduced conduction reserve at elevated heart rates is underscored.

TRANSLATIONAL OUTLOOK: Our findings of reduced conduction reserve in this new, clinically relevant porcine study highlight the need to closely monitor serum potassium levels and heart rate in patients with ischemic heart failure and resistant hypertension.

REFERENCES

1. Smith SM, Gong Y, Handberg E, et al. Predictors and outcomes of resistant hypertension among patients with coronary artery disease and hypertension. J Hypertens 2014;32:635–43.

2. Bapat A, Nguyen TP, Lee JH, et al. Enhanced sensitivity of aged fibrotic hearts to angiotensin II- and hypokalemia-induced early afterdepolarization-mediated ventricular arrhythmias. Am J Physiol Heart Circ Physiol 2012;302:H2331–40.

3. Akar FG, Nass RD, Hahn S, et al. Dynamic changes in conduction velocity and gap junction properties during development of pacing-induced heart failure. Am J Physiol Heart Circ Physiol 2007;293:H1223–30.

4. Akar FG, Rosenbaum DS. Transmural electrophysiological heterogeneities underlying arrhythmogenesis in heart failure. Circ Res 2003; 93:638–45.

5. Akar FG, Spragg DD, Tunin RS, Kass DA, Tomaselli GF. Mechanisms underlying conduction slowing and arrhythmogenesis in nonischemic dilated cardiomyopathy. Circ Res 2004;95: 717–25.

6. Akar FG, Tomaselli GF. Conduction abnormalities in nonischemic dilated cardiomyopathy: basic mechanisms and arrhythmic consequences. Trends Cardiovasc Med 2005;15:259–64.

7. Akar FG, Yan GX, Antzelevitch C, Rosenbaum DS. Unique topographical distribution of M cells underlies reentrant mechanism of torsade de pointes in the long-QT syndrome. Circulation 2002;105:1247–53.

8. Ishikawa K, Ladage D, Tilemann L, Fish K, Kawase Y, Hajjar RJ. Gene transfer for ischemic heart failure in a preclinical model. J Vis Exp 2011;(51). pii: 2778.

9. Ishikawa K, Aguero J, Oh JG, et al. Increased stiffness is the major early abnormality in a pig model of severe aortic stenosis and predisposes to congestive heart failure in the absence of systolic dysfunction. J Am Heart Assoc 2015;4.

10. Boukens BJ, Sulkin MS, Gloschat CR, Ng FS, Vigmond EJ, Efimov IR. Transmural APD gradient synchronizes repolarization in the human left ventricular wall. Cardiovasc Res 2015;108: 188–96.

11. Glukhov AV, Fedorov VV, Kalish PW, et al. Conduction remodeling in human end-stage

nonischemic left ventricular cardiomyopathy. Circulation 2012;125:1835–47.

12. Glukhov AV, Fedorov VV, Lou Q, et al. Transmural dispersion of repolarization in failing and nonfailing human ventricle. Circ Res 2010;106: 981–91.

13. Holzem KM, Gomez JF, Glukhov AV, et al. Reduced response to IKr blockade and altered hERG1a/1b stoichiometry in human heart failure. J Mol Cell Cardiol 2016;96: 82–92.

14. Lang D, Holzem K, Kang C, et al. Arrhythmogenic remodeling of beta2 versus beta1 adrenergic signaling in the human failing heart. Circ Arrhythm Electrophysiol 2015;8:409–19.

15. Lou Q, Fedorov VV, Glukhov AV, Moazami N, Fast VG, Efimov IR. Transmural heterogeneity and remodeling of ventricular excitation-contraction coupling in human heart failure. Circulation 2011; 123:1881–90.

16. Gennari FJ. Hypokalemia. N Engl J Med 1998; 339:451–8.

17. Cooper HA, Dries DL, Davis CE, Shen YL, Domanski MJ. Diuretics and risk of arrhythmic death in patients with left ventricular dysfunction. Circulation 1999;100:1311–5.

18. Siscovick DS, Raghunathan TE, Psaty BM, et al. Diuretic therapy for hypertension and the risk of primary cardiac arrest. N Engl J Med 1994;330:1852–7.

19. Pezhouman A, Singh N, Song Z, et al. Molecular basis of hypokalemia-induced ventricular fibrillation. Circulation 2015;132:1528–37.

20. Shaw RM, Rudy Y. Ionic mechanisms of propagation in cardiac tissue. Roles of the sodium and L-type calcium currents during reduced excitability and decreased gap junction coupling. Circ Res 1997;81:727–41.

21. Wang Y, Rudy Y. Action potential propagation in inhomogeneous cardiac tissue: safety factor considerations and ionic mechanism. Am J Physiol Heart Circ Physiol 2000;278:H1019–29.

22. Moss AJ, Schuger C, Beck CA, et al. Reduction in inappropriate therapy and mortality through ICD programming. N Engl J Med 2012;367: 2275–83.

23. Masson JB, Kovac J, Schuler G, et al. Transcatheter aortic valve implantation: review of the nature, management, and avoidance of procedural complications. J Am Coll Cardiol Intv 2009;2: 811–20.

APPENDIX For a supplemental figure, table, and video, please see the online version of this article.